Polymer/silica core–shell nanoparticles with temperature-dependent stability properties

Clémence Nadal, Olivier Coutelier, Sandrine Cavalie, Valérie Flaud, Jérémy Soulié, Jean-Daniel Marty, Mathias Destarac, Audrey Tourrette

Polymer/silica core-shell nanoparticles with temperature-dependent stability properties

Clémence Nadal[1], Olivier Coutelier[2], Sandrine Cavalie[1], Valérie Flaud[3], Jérémy Soulié[1], Jean-Daniel Marty[2], Mathias Destarac[2*], Audrey Tourrette[1*]

[1] CIRIMAT, Université de Toulouse, CNRS UMR 5085 Université Toulouse III – Paul Sabatier

[2] Laboratoire des IMRCP, Université de Toulouse, CNRS UMR 5623 Université Toulouse III - Paul Sabatier.

[3] ICGM, Univ Montpellier, CNRS, ENSCM

* corresponding authors: destarac@chimie.ups-tlse.fr and audrey.tourrette@univ-tlse3.fr

Highlights

- RAFT synthesis of a triply functional cationic, thermoresponsive and fluorescent PVAm-*b* P(NIPAM-*stat*-NVC) double hydrophilic block copolymer
- Core/shell hybrid nanoparticles assembly with CS/ALG layer-by-layer coating of silica core and further “grafting to” modification with thermoresponsive copolymer
- Temperature-induced destabilization of the hybrid nanoparticles suspension

Abstract

This work aimed at the synthesis of hydrogel-based composite core/shell nanoparticles and their subsequent surface modification with thermoresponsive copolymers. Submicron hydrogel-based nanoparticles were obtained from the layer-by-layer coating of silica nanoparticles with two natural oppositely-charged polyelectrolytes, chitosan and sodium alginate. Further modifications with a PVAm-*b*-PNIPAM copolymer synthetized by RAFT polymerization was achieved by the “grafting to” approach. First, the optimum feed weight ratio (fwr) was determined by a combined approach of zeta potential and T2 relaxation time measurements. Then, diblock grafting at this optimum fwr was performed and characterized by XPS. XPS analysis confirmed the presence of copolymer at the particles’ surface with the increase of C and N atomic percentage. The quantification study was carried out by spectrofluorimetry using the fluorescently labeled PVAm-*b*-P(NIPAM-*stat*-NVC) copolymer and revealed that the grafting efficiency could reach 60 %. Finally, a study of thermosensivity properties study confirmed that our smart system allowed a temperature-induced destabilization of the particles suspension at 45 °C. This work has promising prospects in the field of controlled drug delivery.

Keywords

Thermoresponsive polymers, RAFT polymerization, core/shell nanoparticles, surface modification, grafting to, biopolymers

Graphical abstract

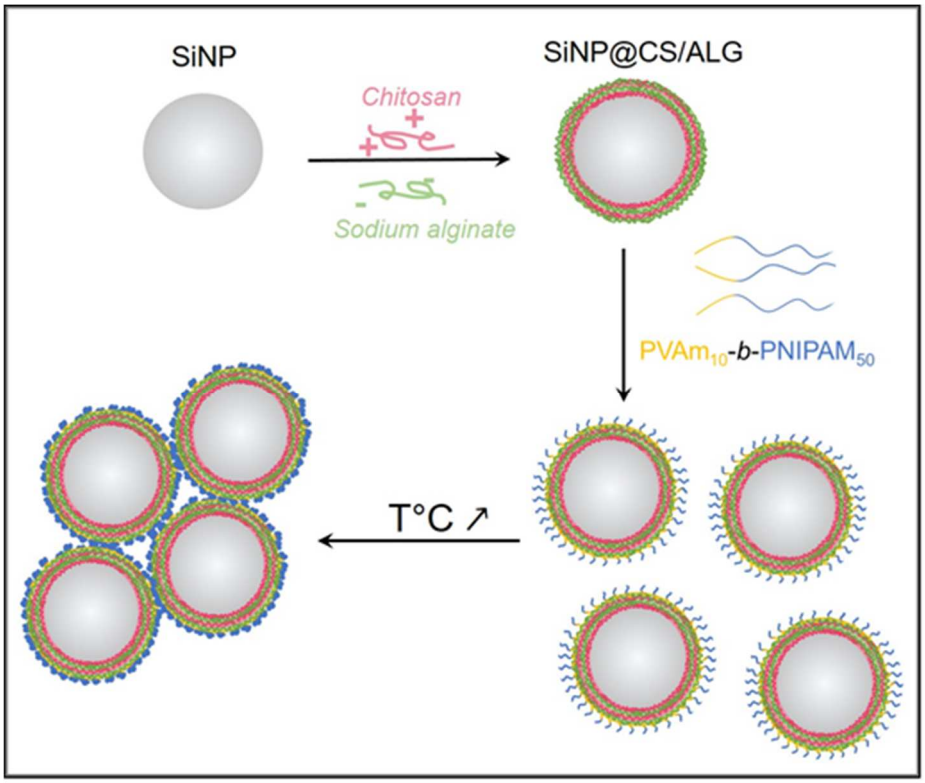

Introduction

Micro- and nanoparticles have long been used in biomedical applications as drug delivery vehicles for diagnostics, treatment in various diseases including tumor, as well as in tissue engineering.[1–3] These particles possess some advantages compared to particles in the macroscale and bulk materials due to their higher surface to volume ratio.[4,5] Stimuli-responsive particles are particularly interesting because of their ability to change their structure, conformation or size in response to internal and/or external stimuli that help the controlled release of drugs, stability, bioadhesion, etc.[6,7] A large range of stimuli can be used to control physico-chemical properties of these systems including pH, temperature, redox, light, magnetic, electrochemical potential, glucose, enzyme, microwave, ultrasonic and ionic strength.

The use of polymers to coat particles is an area of growing interest to create smart core-shell particles.[8–10] This type of design provides the opportunity to tune the resulting nanocomposite material that exhibits specific characteristics of the core depending on its nature (polymer, hydrogel, silica, metal...) such as size, porosity, degradability, and those of the shell such as stimuli-responsiveness.[11] Polymer-coated particles are generally prepared by either adsorption of chains onto the surface or by covalent bonding according to "*grafting to*" or "*grafting from*" approaches.[12]

Among the polymer surface modification methods, the *layer-by-layer* (LbL) assembly has been widely used to fabricate responsive particles with tunable architectures and properties. This technique simply involves the alternating deposition of oppositely charged polymers onto surfaces.[13] This method has been used to prepare pH-responsive drug delivery systems based on silica nanoparticles.[14] Polyelectrolyte multilayers of alginate/chitosan natural polymers were assembled on mesoporous silica nanoparticles surface to act as pH-sensitive and biocompatible shell layer.[15] The anticancer drug Doxorubicin release from these nanocarriers was pH dependent, and *in vivo* biodistribution study showed that drug-loaded nanocarriers had longer systemic circulation and slower plasma elimination than the free drug. Alginate and chitosan polysaccharides have been coated on different silica particles by LbL method to provide pH-controlled drug release.[16]

Polymer coating of particles can also be achieved to control particle–particle interactions and consequently colloidal stability.[17,18] Hence, when the particles are coated with a stimuli-responsive polymer, stable, well-dispersed systems can be switched to aggregation-prone ones.[19,20] Poly(N-isopropylacrylamide) (PNIPAM) is a commonly used polymer to introduce temperature responsiveness onto particles surface. Indeed, PNIPAM undergoes a phase transition from a hydrophobic to a hydrophilic state when the external temperature is equal to a lower critical solution temperature (LCST) of about 32°C in aqueous solution.[21] This phase transition is mainly related to the disruption

above LCST of hydrogen bonds between amide groups and water molecules in favor of hydrogen bonds between amide groups owing to different PNIPAM chains. This also reinforces the hydrophobic character of PNIPAM chains that are prone to aggregate in solution above LCST.

PNIPAM-based block copolymers are especially interesting since they can be multi-responsive depending on the nature of the other block.[22] pH-Responsive PNIPAM-based copolymers, such as poly(acrylic acid)-*b*-poly(*N*-isopropylacrylamide) (PAA-*b*-PNIPAM)[23] or poly(2-(dimethylamino)ethyl acrylate)-*b*-poly(*N*-isopropylacrylamide) (PDMAEA-*b*-PNIPAM)[24] copolymers, are often reported in drug delivery applications. Another pH-sensitive polymer, poly(vinyl amine) (PVAm), generated curiosity of multiple research teams. However, as simple as its structure may seem, its synthesis is in fact not trivial. PVAm was described by Pelton *et al*.,[25] which reported a polymer displaying a high primary amine content, a good solubility over a large range of pH (2-11) and a polyelectrolyte behaviour. Synthesis of PVAm by free radical polymerization was described for the first time in 1947[26] and optimized since, until industrial development. However, when it comes to low dispersities and controlled average molar masses, the lack of representation of PVAm in the literature highlights how its synthesis via reversible-deactivation radical polymerization (RDRP) is still a challenge. Debuigne and coworkers reported organometallic mediated radical polymerization as one of the most adapted technology to access poly(vinyl amine) with controlled macromolecular characteristics[27] and used it to polymerize N-vinyl acetamide with a cobalt complex as transfer agent, followed by acidic hydrolysis of acetamide pendant groups into primary amines. However, cobalt chemistry displays its flaws as any technology and its high-level technicity tends to prevent easy access. A Japanese team led by Mori reported for the first time RDRP of PVAm using reversible addition-fragmentation chain transfer (RAFT) polymerization.[28] Their approach was based on the polymerization of N-vinylphthalimide (NVPI) followed by the deprotection of phtalimido with hydrazine and was used to perform the synthesis of various PVAms, namely homopolymer, predominantly alternating copolymer with NIPAM[29] and block copolymer such as PVAm-*b*-PNIPAM.[30] The latter copolymer possess a cationic character and was especially studied for its ability to interact with anionic polymers such as DNA.[30,31] The amine functions of PVAm are also suitable candidates for covalent reactions with carboxylic acids by peptide coupling.[32] Such a surface modification performed with PVAm-*b*-PNIPAM copolymer would allow the creation of an original multi-layered smart system with advanced surface properties: a stability depending on temperature conditions.

In that context, our work aimed at the formation of core/shell silica/hydrogel composite nanoparticles with a thermosensitive outer shell. For this, as depicted in Scheme 1, a silica core nanoparticle (SINP) was first wrapped with a polyelectrolyte multilayer made of chitosan/alginate polymers deposited using a layer-by-layer strategy (SiNP@CS/ALG, Step 1). A further modification with a PVAm-*b*-PNIPAM

copolymer synthesized by RAFT polymerization (Step 2) was achieved by the "grafting to" approach (Step 3). Although SiNP@CS/ALG were already described in the literature,[14,15] the modification of their surface with thermoresponsive polymers such as PVAm-*b*-PNIPAM and the study of their stability in response to temperature were as far as we know never reported. In this work, surface modifications of silica NPs were studied through thermogravimetry, XPS and fluorescence measurements. For this the fluorescent N-vinylcarbazole (NVC) probe was used as comonomer for the synthesis of original PVAm-*b*-P(NIPAM-*stat*-NVC) block copolymer.[33] Thermoresponsive and stability properties were further studied by means of scattering measurements.

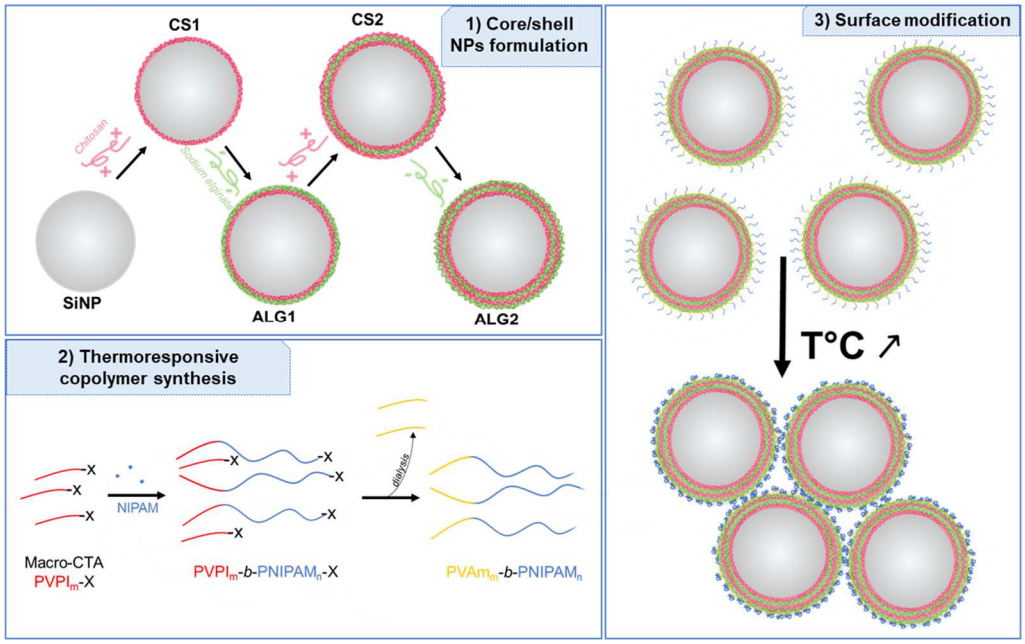

Scheme 1 Elaboration of thermoresponsive surface-modified SiNP@CS/ALG nanoparticles in a three steps process.

Experimental section

1. Materials

1.1. Polymer synthesis.

N-Vinylphthalimide (NVPI, 99%, Acros Organics), N-isopropylacrylamide (NIPAM, 97%, Aldrich), hydrazine monohydrate (98%, Sigma Aldrich), dilauryol peroxide (LPO, 99%, Acros Organics), methanol (99.9%, Sigma-Aldrich), N-N-dimethylformamide (DMF, 99.9%, Sigma-Aldrich), diethyl ether (99.9% Sigma-Aldrich), 1,4-dioxane (VWR) were used as received. 2,2-Azobisisobutyronitrile (AIBN, 98%, Acros Organics) was purified by recrystallization from methanol. *O*-ethyl-*S*-(1-methoxycarbonyl)ethyldithiocarbonate (RAFT agent, xanthate XA1) was synthetized following a previously reported method.[34] Ultrapure water from obtained from a Elga Purelab Flex device with

resistivity value under 18 MΩ/cm. Dialysis were carried in 1 kDa cut-off dialysis tubes from GE Healthcare Bio-Sciences Corp.

1.2. Nanoparticles formulation.

Absolute ethanol, ammonium hydroxide (NH_4OH, 20 %), sodium hydroxide (NaOH), sodium chloride (NaCl) and chlorhydric acid (HCl) were obtained from Thermofisher and used as received. Tetraethyl orthosilicate (TEOS), acetic acid, dimethylsulfoxide (DMSO), N-(3-Dimethylaminopropyl)-N'-ethylcarbodiimide (EDC), N-hydroxysuccinimide (NHS) were provided by Sigma Aldrich and used as received. Finally, biopolymers chitosan (CS, batch #STBH6262, Mv 770 kDa, deacetylation degree 75 %) and sodium alginate (ALG, batch #058K0126, Mv 150 kDa, M/G ratio 2.4) were supplied from Sigma Aldrich and characterized by NMR and viscosimetry.

2. Polymer synthesis

2.1. RAFT polymerization of macro-chain transfer agent $PVPI_{10}$-X.

The synthesis of macro-chain transfer agent (macro-CTA) was adapted from Mori *et al.*[28] A typical RAFT polymerization procedure is the following: in a Schlenk tube were introduced N-vinylphthalimide (1.39 g, 8.0 mmol), xanthate XA1 (153.7 mg, 0.74 mmol), AIBN (19.2 mg, 0.12 mmol) and DMF (4 mL). The mixture was degassed by four freeze-pump-thaw cycles, backfilled with argon then introduced in an oil bath at 60 °C for 24 h. The reaction was stopped by cooling it down with liquid nitrogen. A sample of the pale-yellow crude mixture was collected for analysis by ^{1}H-NMR in DMSO-d6 to determine monomer conversion. Finally, the obtained polymer was precipitated in diethyl ether, filtered off and dried under vacuum. A white powder was recovered. SEC analysis and ^{1}H-NMR were carried out to determine respectively $M_{n,\mathrm{MALS}}$ and $M_{n,\mathrm{NMR}}$ values. ($M_{n,\mathrm{NMR}}$ = 2300 g mol^{-1}, $M_{n,\mathrm{MALS}}$ = 2700 g mol^{-1}, $Đ$ = 1.1)

2.2. RAFT synthesis of $PVPI_{10}$-b-$PNIPAM_{50}$-X and $PVPI_{10}$-b-P(NIPAM-stat-$NVC)_{50}$-X copolymers.

A typical RAFT block copolymerization procedure is the following: in a Schlenk tube were introduced NIPAM (2 g, 17.7 mmol), previously synthetized $PVPI_{10}$-X (686 mg, 0.35 mmol), AIBN (12 mg, 0.07 mmol) and DMF (4 mL). The mixture was degassed by four freeze-pump-thaw cycles, backfilled with argon then introduced in an oil bath at 65 °C for 16 h. The reaction was stopped by cooling it down with liquid nitrogen. Monomer conversion was determined by ^{1}H-NMR in DMSO-d6 analysis. Finally, $PVPI_{10}$-b-$PNIPAM_{50}$-X polymer was precipitated in diethyl ether, filtered off and dried under vacuum. A white powder was recovered. SEC analysis and ^{1}H-NMR were carried out to determine respectively $M_{n,\mathrm{MALS}}$ and $M_{n,\mathrm{NMR}}$ values. ($M_{n,\mathrm{NMR}}$ = 7900 g mol^{-1}; $M_{n,\mathrm{MALS}}$ = 6900 g mol^{-1}; $Đ$ = 1.72). From this method were also synthetized copolymers with structure $PVAm_m$-*b*-P($NIPAM_{1-x}$-*stat*-$NVC_x)_n$ with m and n the number-average degree of polymerization of each block, and x the molar fraction of NVC in the statistical second block. In the case of $PVPI_{10}$-*b*-P($NIPAM_{0.92}$-*stat*-$NVC_{0.08})_{50}$-X copolymerization, the

protocol was adapted from Suchao-in *et al.*[33] and 8% mol of NVC with respect to NIPAM were introduced within the Schlenk tube and the amount of CTA was adjusted to maintain a theoretical DP_n of 50. The rest of the procedure was kept unchanged.

Kinetic studies were carried out using the same protocol. Samples were collected at defined times with degassed syringes and immediately cooled down in liquid nitrogen. A fraction was analyzed by ^{1}H-NMR to determine monomer conversion and the remaining sample was analyzed by SEC to determine $M_{n,\mathrm{MALS}}$ values.

2.3. Elimination of the xanthate chain-end functionality

Removal of chain-end xanthate was carried out according to a previously reported procedure[35] as follows: typically, $PVPI_{10}$-*b*-$PNIPAM_{50}$-X copolymer (2 g, 0.41 mmol), dilauroyl peroxide (65 mg, 0.16 mmol), propan-2-ol (28 mL) were introduced in a Schlenk tube. The mixture was degassed by four freeze-pump-thaw cycles, backfilled with argon and heated at 80 °C in an oil bath. The mixture was stirred for 10 h during which 1 mL of a degassed dilauryol peroxide (130 mg, 0.33 mmol) solution in propan-2-ol (4 mL) was introduced every two hours. The mixture was allowed to return to room temperature, then propan-2-ol was evaporated under vacuum. The resulting oil was dissolved in a small amount of DMF. The copolymer was precipitated in diethyl ether, filtered off and dried under vacuum. $M_{n,\mathrm{MALS}}$ = 9000 g mol^{-1}; $Đ$ = 1.40

2.4. Hydrazinolysis of PVPI to PVAm

Hydrazinolysis procedure was adapted from Mori *et al*.[28] and carried out as follows: in a round-bottom flask was dissolved $PVPI_{10}$-*b*-$PNIPAM_{50}$ copolymer (1.05 g, 0.646 mmol phthalimide units) in 12 mL of a methanol/dioxane mixture with a 2/1 volume ratio. Hydrazine monohydrate (646 mg, 12.9 mmol) was introduced and the mixture degassed by bubbling of argon for 1 h. The flask was equipped with a reflux condenser connected to argon and the mixture was carried to reflux (85 °C) for 6 h. Heating was stopped and solvents removed under vacuum. The resulting oil was dissolved in MeOH/aqueous HCl (0.5M) in 2/1 volume ratio. $PVAm_{10}$-*b*-$PNIPAM_{50}$ was finally precipitated in diethyl ether, filtered off, dried under vacuum and dialyzed at pH > 9 against ultrapure water for 4 days. The same procedure was adapted for the hydrazinolysis of $PVPI_{10}$-*b*-P(NIPAM-*stat*-$NVC)_{50}$ into $PVAm_{10}$-*b*-P(NIPAM-*stat*-$NVC)_{50}$. Final copolymers were recovered by lyophilization and used as such for the nanoparticles surface modification.

3. Nanoparticles elaboration

3.1. SiNP nanoparticles

Silica nanoparticles (SiNP) were prepared according to a reported method based on a modified-Stöber sol/gel process.[36,37] Typically, absolute ethanol (100 mL) was mixed with milli-Q water (10.8 mL)

and NH_4OH solution (3.9 mL) under vivid agitation for 15 minutes. TEOS (6.3 mL) was added to the mixture in one-shot. After 17 h at room temperature, particles were filtered onto 0.2 µm cellulose nitrate membrane filters (Whatman), frozen with liquid nitrogen and lyophilized.

3.2. SiNP@CS/ALG nanoparticles

SINP@CS/ALG nanoparticles were obtained by *LbL* modification of SiNP nanoparticles according to Feng *et al*. and Du *et al*..[14,15] Typically, a SiNPs suspension at 50 mg mL^{-1} (8 mL, 400 mg SiNPs) was prepared by ultrasonication, cooled down and added to chitosan (CS) solution at 10 mg mL^{-1} (400 mL, 4 g CS) in acetic acid solution at 1%$_{v/v}$. The suspension was under vivid agitation for 17 h at room temperature. CS1 particles were collected by centrifugation (15 000 g/10 min) and washed twice with water. CS1 nanoparticles were suspended in water at 3.3 mg mL^{-1}, a sample was collected for characterization. A sodium alginate solution at 1 mg mL^{-1} was added to CS1 suspension. The mixture was agitated at room temperature for 1 h. ALG1 particles were collected by centrifugation (15 000 g/10 min) and washed twice with water. ALG1 nanoparticles were suspended in water at 3.3 mg mL^{-1}, a sample was collected for characterization. This last step was replicated twice with a chitosan solution at 1 mg mL^{-1} in acetic acid 1%$_{v/v}$ to obtain CS2 nanoparticles, then with a sodium alginate aqueous solution at 1 mg mL^{-1} to obtain ALG2 (SiNP@CS/ALG) final nanoparticles.

3.3. Nanoparticles surface modification

Typically, 100 mg SiNP@CS/ALG nanoparticles at 5 mg mL^{-1} (in water or in DMSO) were introduced in a reactor. $PVAm_m$-*b*-P(NIPAM-*stat*-$NVC)_n$ solution at 1 mg mL^{-1} (in water or DMSO) was added at 1% weight ratio with regard to the nanoparticles. EDC and NHS solutions at 10 mg mL^{-1} in DMSO were added with molar equivalents *eq* COOH: *eq* EDC : *eq* NHS = 1 : 4 : 2. The suspension was agitated for 24 h at room temperature the grafted particles were collected by centrifugation (15 000 g during 10 minutes) and washed twice with water. To determine optimal feed weight ratio, samples at different feed weight ratios from 0 to 5 %$_{wt}$ were prepared according to the previously described procedure.

4. Characterizations

4.1. Refractive index increment (dn/dc)

dn/dc value of poly(vinyl phthalimide) was measured on a refractive index detector DnDc 2012 PSS thermostated at 35 °C, at a wavelength of 620 nm using DMF-LiBr (10 mM) eluent. A dn/dc equal to 0.153 mL g^{-1} was found for PVPI in such conditions. In the case of PVPI-*b*-PNIPAM, dn/dc value was determined from the empirical linear relation: $dn/dc_{(A\text{-}block\text{-}B)} = F_A*(dn/dc)_A + F_B*(dn/dc)_B$ with F_A and F_B the weight fractions respectively of block A and block B. By using reported dn/dc value of PNIPAM in DMF-LiBr (10 mM) i.e. 0.087 mL g^{-1} [38], a value of refractive index increment equal to 0.103 mL g^{-1} was found for PVPI-*b*-PNIPAM.

4.2. Size Exclusion Chromatography (SEC)

Samples were prepared in DMF-LiBr (10 mM) at 5 mg mL^{-1} and filtered on a PTFE 0.45 µm filter. SEC injections were performed with a 1.0 $mL.min^{-1}$ flow rate on a Dionex UltiMate 3000 UHPLC pump from Thermo Scientific equipped with two Tosoh columns (α-2500, 8.0 x 300 mm and α-3000, 8.0 x 300 mm). Columns were thermostated at 55 °C in an oven. Multi-detection was provided from a refractive index detector (RI) Wyatt Optilab rEX, a UV detector Varian ProStar 325 UV and a multi-angle light scattering (MALS) detector Wyatt MiniDawn TREOS. Average molar masses and dispersities were determined from RI-MALS analysis. All data were processed with Astra7 software from Wyatt Technology.

4.3. Nuclear Magnetic Resonance (NMR).

^{1}H-NMR spectra of polymer samples were recorded at 300.13 MHz on a Bruker Advance 300 MHz spectrometer. DOSY NMR spectra were recorded on a Bruker Advance 500 MHz spectrometer equipped with a cryoprobe. DMSO-d6 was used for all PVPI-containing samples, D_2O was used for PVAM-based copolymers. T2 relaxation (low field NMR) measurements were performed on nanoparticle samples with an Acorn Area device from Xigo Nanotools. Dried nanoparticles were suspended at different concentrations (0.5 – 1 - 1.5 - 2 $\%_{wt}$) in 1 mM KCl aqueous solution. T2 relaxation times measurements were performed at each concentration after agitation and sonication of the samples. 6 runs were carried out for each measurement.

4.4. Dynamic Light Scattering (DLS) and Zeta potential measurements.

Size and ζ-potential measurements of core/shell nanoparticles were acquired on a Malvern ZetaSizer Nano ZS with a He-Ne laser at 633 nm. 120 s equilibration time was applied then 3 measurements were performed with 15 runs of 10 s. Intensity-weighted mean hydrodynamic diameters (Z-av) were obtained from DLS from cumulant analysis as well as polydispersity indexes (PDI). Samples were prepared at 0.5 mg mL^{-1} in ultrapure water.

Feed weight ratio of the surface modification process was characterized using ζ-potential measurements performed on a WALLIS$^{\zeta}$ device from Cordouan Technologies.

4.5. Thermogravimetric analysis (TGA)

TGA was performed on a Setaram TAG16 apparatus. Samples were heated under Argon flow from 25 °C to 700 °C with a 5 °C min^{-1} heating rate.

4.6. Transition electronic microscopy (TEM)

TEM images were acquired on a Hitachi HT7700 device. Samples were prepared by depositing cupper carbon grids (FCF400-CU from Electron Microscopy Sciences) on a drop of the suspension (0.5 mg mL^{-1}) to analyze. After 5 minutes, the residual suspension was removed by blotting with a filter paper.

4.7. X-ray photoelectron spectroscopy (XPS)

XPS measurements were performed on an ESCALAB 250 device from Thermo Electro. Excitation source was monochromatic with Al Kα line (1486.6 eV). Analyzed surface displayed a diameter of 500 µm. The background signal was removed using the Shirleymethod.[39] The surface atomic concentrations were determined from photoelectron peaks areas using the atomic sensitivity factors reported by Scofield.[40] Photoelectron spectra were calibrated in bonding energy, with respect to C-C contribution in C1s orbital at 284.8 eV. Charge was compensated with an electron beam (-2 eV).

4.8. Spectrofluorimetry

Spectrofluorimetry was performed on a Fluorolog Horiba iHR320 device. Emission mode was used to record spectra. Excitation was set at 325 nm and the splits were 1.5 nm for both excitation and emission. Corrected signals S1c/R1c were plotted.

4.9. Colloidal stability

Colloidal stability was investigated with TurbiscanLab from Formulaction (France). Grafted and non-grafted nanoparticles suspensions at 10 mg mL^{-1} in 10^{-3} M NaCl were studied at 25 °C and 45 °C. Samples were introduced in the device to stabilize at a defined temperature, then dispersed by vortexing and analysis were launched. Total duration of measurement was 30 min, with scans acquired every 1 min 15 seconds.

Results and discussion

A 3-steps strategy was followed to design our smart system as depicted in Scheme 1. First, composite SiNP@CS/ALG core/shell nanoparticles were designed by layer-by-layer deposition of polyelectrolyte multilayer around a silica core (Step 1). The surface modification of SiNP@CS/ALG nanoparticles required the use of LCST PVAm-*b*-PNIPAM diblock copolymers that were synthesized by RAFT polymerization (Step 2). In order to monitor surface modification, the copolymer composition was adjusted to act as a fluorescent probe by copolymerizing fluorescent NVC monomer with NIPAM to obtain PVAm-*b*-P(NIPAM-*stat*-NVC). Finally, the nanoparticles' surface modification was achieved by the "grafting to" approach applied to PNIPAM-based copolymers, followed by characterization and grafting quantification (Step 3).

1. Core/shell nanoparticles elaboration and characterization

Silica nanoparticles (SiNP) were synthetized from a modified-Stöber sol/gel process in alkaline media.[36] Tetraethylorthosilicate (TEOS) precursor was poured in a mixture of absolute ethanol and ammonia solution resulting in hydrolysis and condensation of TEOS silanol groups, thus forming spherical nanoparticles. In this work, parameters such as pH and TEOS concentration were reproduced according to Lagarrigue *et al.* to obtain submicron monodisperse nanoparticles.[37] Hydrodynamic diameter Dh (Z-av) determined by DLS was 359 nm, number- and intensity distributions of Dh (Fig. SI1) were narrow, confirming an efficient sol/gel process.

SiNP@CS/ALG core/shell nanoparticles were obtained by coating the silica core with a hydrogel shell. An assembly of oppositely charged chitosan and sodium alginate polyelectrolytes was built with LbL deposition technique.[13] Two polycation/polyanion bilayers were successively deposited, they will be referred to as CS1, ALG1, CS2 and ALG2 in the following. LbL assembly construction was followed with ζ-potential measurements as displayed in Fig. 1a and by thermogravimetric analysis (Fig. 1b).

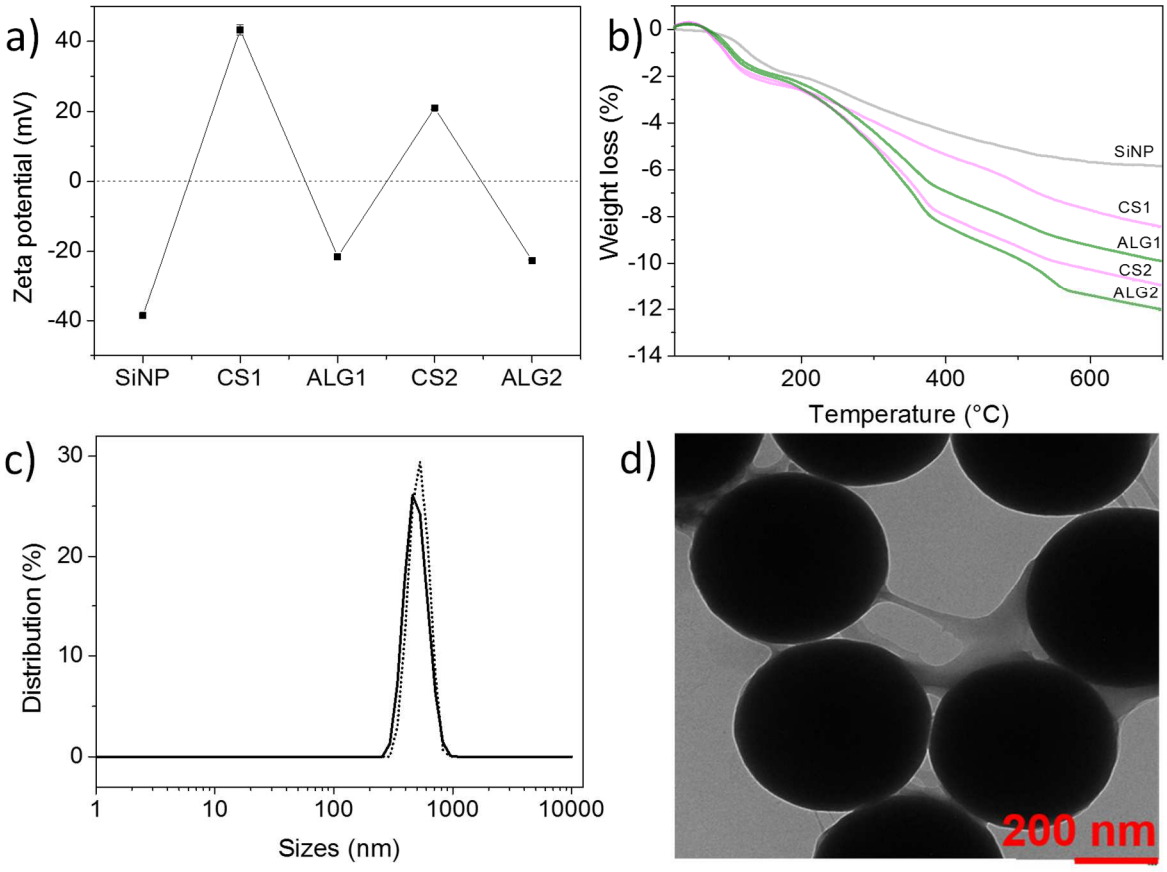

Fig. 1 a) Zeta potential measurements at each layer of the LbL process. pH were comprised between 6.3 and 6.8 (error bars are hidden by mean values marks) b) TGA thermograms of core/shell nanoparticles obtained at different step of LbL process with a heating rate equal to 5 °C min^{-1} c) Intensity-averaged (dotted line) and number-averaged (plain line) distributions of hydrodynamic diameters of SiNP@CS/ALG nanoparticles measured in water at 0.5 mg mL^{-1}; d) TEM image of SiNP@CS/ALG.

Starting from negative zeta potential of pristine silanol surfaces, ζ-potentials went from successively positive values when chitosan was the outer layer to negative ones when alginate was on the outer surface (Fig. 1a). This alternation strongly suggests the success of the LbL strategy. As showed in Fig. 1b, the TGA thermogram of nanoparticles at every step of the LbL deposition confirmed this with a weight loss increasing constantly with the number of layers. From these TGA measurements, a final polymer/SiNP ratio can be estimated at 6%$_{wt}$. TEM images of final SiNP@CS/ALG nanoparticles highlighted the presence of an organic corona around inorganic cores as shown in Fig. 1d. Finally, a mean hydrodynamic diameter (Z-av) of 474 ± 95 nm was estimated for SiNP@CS/ALG nanoparticles in solution (Fig. 1c). From DLS measurements, the thickness of the hydrogel corona was then roughly estimated to 50 nm.

2. Synthesis of block copolymers of vinyl amine and N-isopropylacrylamide

The synthesis of poly(vinyl amine)-*b*-poly(N-isopropylacrylamide) copolymers was achieved with controlled molar mass and well-defined structure PVAm$_m$-*b*-PNIPAM$_n$, with m and n the number-average degree of polymerization of each block. We followed a two-step RAFT polymerization strategy

based on the work of Mori and coworkers [28,30] with a first RAFT polymerization of NVPI in presence of xanthate XA1, to form a xanthate-capped PVPI ($PVPI_m$-X). $PVPI_m$-X was used as macro-CTA in a second RAFT polymerization of NIPAM to afford $PVPI_m$-*b*-$PNIPAM_n$-X. The terminal xanthate functionality was removed by radical reaction with dilauroyl peroxide in propan-2-ol leading to a $PVPI_m$-*b*-$PNIPAM_n$ copolymer. Finally, $PVPI_m$-*b*-$PNIPAM_n$ was reacted with an excess of hydrazine and converted into a $PVAm_m$-*b*-$PNIPAM_n$. (Scheme 2).

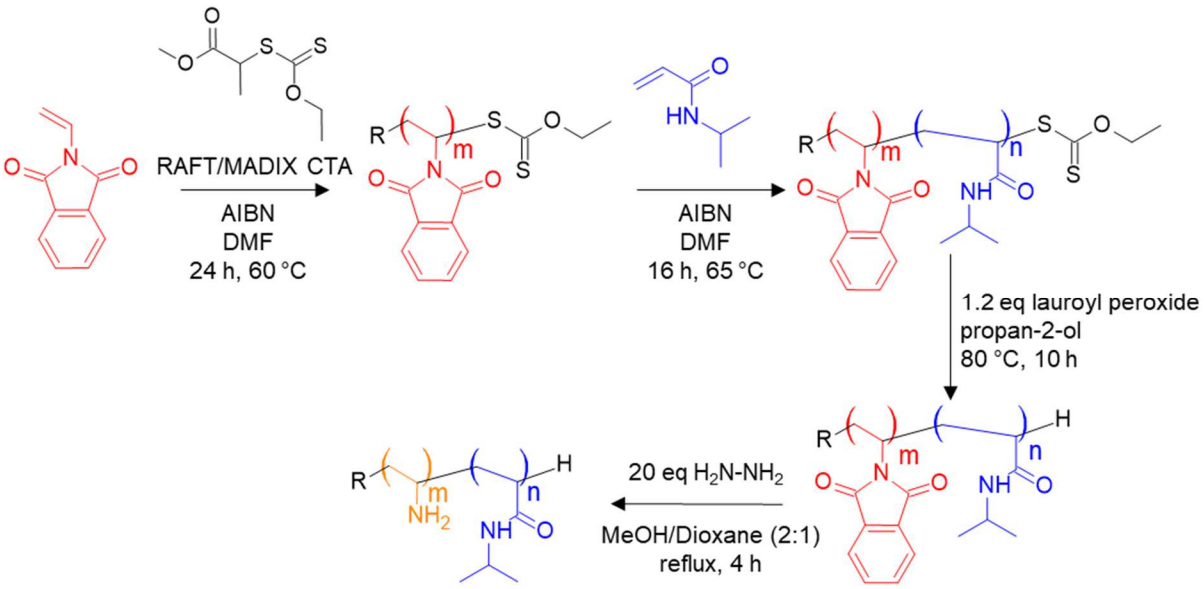

Scheme 2 General scheme for the synthesis of PVAm-b-PNIPAM copolymers

PVPI-*b*-PNIPAM copolymer with targeted structure $PVPI_{10}$-*b*-$PNIPAM_{50}$-X was selected. The synthesis of PVPI block was obtained with a NVPI conversion of 80% (Fig. SI2). Number-average molar mass measured by SEC, $M_{n,MALS}$ = 2300 g mol^{-1} for $PVPI_{10}$-X, was slightly overestimated but still in good agreement with the theoretical one ($M_{n,th}$ = 1700 g mol^{-1}). Dispersity (***Đ***) of 1.06 attested a good level of control of the first block. (Entry 1,Table 1).

Table 1 Details of block copolymer synthesis from PVPI-X macro RAFT agent

Entry	Sample	Targeted DP_n	Targeted M_n (g/mol)	Monomer conversion[a] (%)	$M_{n,th}$[b] (g/mol)	$M_{n,MALS}$[c] (g/mol)	*Đ* [c]
1	PVPI-X	10	2000	80	1700	2300	1.06
2	PVPI-*b*-PNIPAM-X	50	7700	> 98	7650	7500	1.26

3	PVPI-*b*-P(NIPAM-*stat*-NVC)-X	50	8000	> 97	8000	10000	1.41

[a] determined from ^{1}H-NMR spectrum of crude mixture; [b] theroretical M_n calculated as $M_{n,th}$ = $[M]_0/[CTA]_0$*conv*M_M+M_{CTA} ; [c] determined from SEC-RI-MALS data with dn/dc PVPI = 0.153 mL g^{-1}and dn/dc PVPI-*b*-PNIPAM = 0.103 mL g^{-1}

$PVPI_{10}$-X was used as macro-CTA in NIPAM polymerization to form thermoresponsive copolymer $PVPI_{10}$-*b*-$PNIPAM_{50}$-X. A kinetic study of the copolymerization was carried out over 10 hours in DMF at 65 °C. The evolution of NIPAM conversion with time and the evolution of M_n and dispersity with respect to NIPAM conversion are displayed respectively in Fig. 2a and Fig. 2b. Fig. 2a shows a fast rate of polymerization. Indeed, NIPAM conversion reached 50 % in 30 minutes and was nearly quantitative after 10 hrs (> 98 %), as expected for a NIPAM polymerization controlled by RAFT with a xanthate.[41] The M_n of the resulting block copolymer displayed in Fig. 2b increased linearly with conversion and the dispersity remained below 1.3 throughout the polymerization, suggesting that the macro-CTA $PVPI_{10}$-X efficiently controls the copolymerization of NIPAM in such reaction conditions.

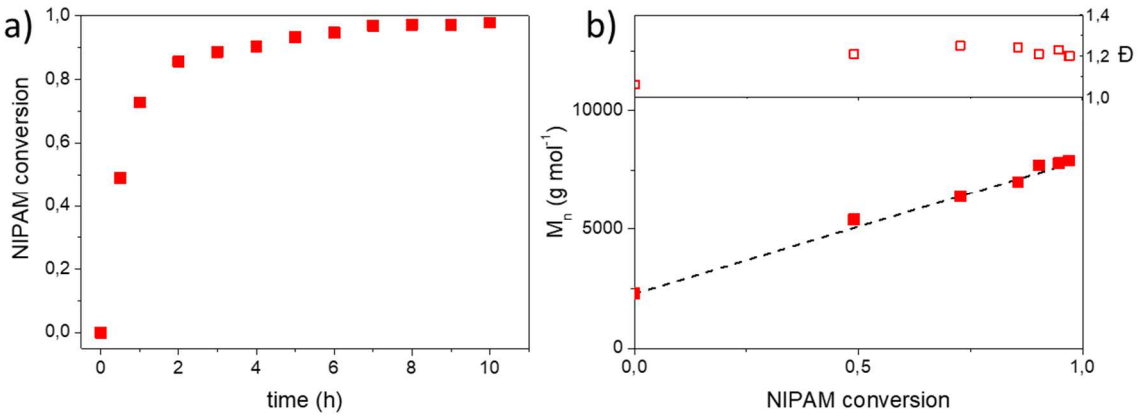

Fig. 2 Evolution of (a) NIPAM conversion in time, (b) M_n and dispersity with respect to NIPAM conversion. Reaction conditions: $[NIPAM]_0/[PVPI_{10}\text{-}X]_0/[AIBN]_0$ = 50/1/0.2, T = 65 °C, DMF as solvent.

Chain extension was confirmed by SEC analysis, although the SEC-RI trace of the final copolymer revealed the presence of unreacted PVPI (Fig. 3a).

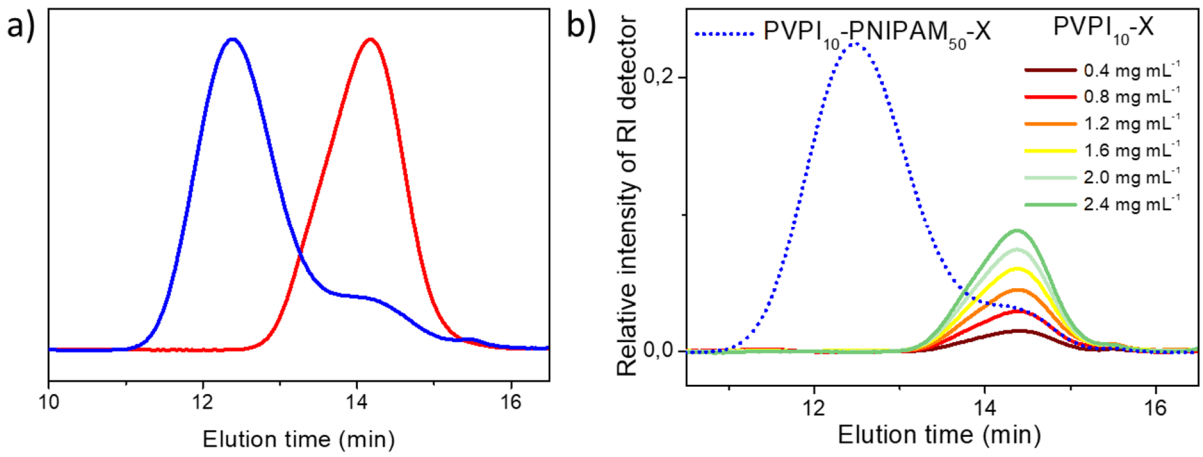

Fig. 3 a) Overlay of SEC-RI chromatograms of $PVPI_{10}$-X macro-CTA (red) and $PVPI_{10}$-$PNIPAM_{50}$-X (blue) after 98 % NIPAM conversion. b) Estimation of the amount of unreacted $PVPI_{10}$-X (23 min elution) after diblock formation through calibration with $PVPI_{10}$-X samples at different concentrations (see calibration curve in Fig. SI4).

NIPAM polymerization in presence of $PVPI_{10}$-X macro-CTA was followed by SEC-UV analysis at 254 nm to selectively observe the evolution of the UV-absorbing PVPI block during polymerization (Fig. SI3). After 98% NIPAM conversion, the SEC-UV signal clearly showed a double distribution, indicating the presence of PVPI in final block copolymer together with a non-negligible amount of unreacted $PVPI_{10}$-X. The evolution of the SEC-UV traces with time (Fig. SI3) clearly indicated a slow reactivity of the first $PVPI_{10}$-X block, whose concentration gradually decreases with time in favor of the formation of the corresponding diblock copolymer. To estimate the fraction of residual first block in the mixture, a calibration curve of $PVPI_{10}$-X was drawn with the maximum intensity of $PVPI_{10}$-X SEC-RI signal plotted against its concentration from 0.4 to 2.4 mg mL^{-1}, as detailed in Fig. S4. Then, the intensity of PVPI-X trace was determined on the SEC-RI signal of $PVPI_{10}$-*b*-$PNIPAM_{50}$-X and correlated to a concentration of 0.8 mg mL^{-1} of $PVPI_{10}$-X, as shown in Fig. 3b. This allowed an estimation of the residual first block at 16 %wt in the copolymer/homopolymer mixture, corresponding to a fraction of 60 % unreacted macro-CTA.

Hence taking into account this incomplete block copolymer formation, the recalculated theoretical DP_n of PNIPAM block in PVPI-*b*-PNIPAM-X copolymer should be equal to 90 instead of 50. First interrogation would be whether these 60 % of $PVPI_{10}$-X chains were still terminated by xanthate function. This could not be verified since the presence of terminal xanthate is usually confirmed with SEC-UV at its characteristic wavelength of 290 nm but PVPI absorbs in UV range from 250 nm to 315 nm, hiding any contribution of xanthate. However, these results suggest a low transfer constant C_{tr} of our macro-RAFT agent in NIPAM polymerization, as reported by Mori.[30] In order to avoid diblock contamination by PVAm homopolymer, the copolymer was purified by dialysis after hydrazinolysis.

Prior to deprotection of phthalimide units by hydrazine, a radical reduction of the terminal xanthate group with dilauroyl peroxide was performed according to a previously reported method,[34] to avoid the formation of thiol-ended chains during hydrazinolysis that could end up in the formation of triblock copolymers by oxidation of the thiols into disulfides.[42] Hydrazinolysis of PVPI blockwas carried out in large excess of hydrazine with respect to phthalimide (20: 1 molar). After 6 hours refluxing in a methanol/dioxane (2:1) mixture at 85 °C, ^{1}H-NMR showed the disappearance of the signals of the aromatic protons (Fig. 4) as expected.[28]

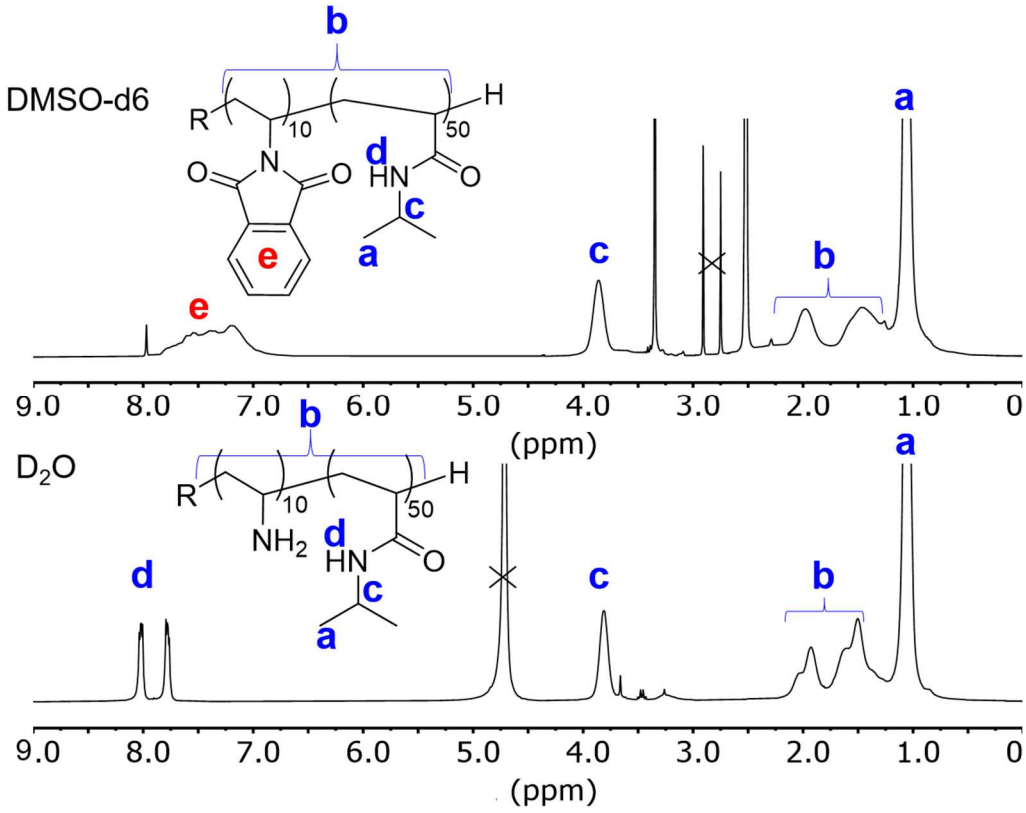

Fig. 4 ^{1}H-NMR spectra of (up) $PVPI_{10}$-b-$PNIPAM_{50}$ in DMSO-d6 and (bottom) $PVAm_{10}$-b-$PNIPAM_{50}$ in D_2O

M_n value of final copolymer was determined theoretically knowing the initial DP_n of PVPI-X (11), the molecular weight of VAm units and the DP_n of the second block (64) and equalled M_n = 7700 g mol^{-1} for $PVAm_{10}$-*b*-$PNIPAM_{50}$.

A fluorescent homologous poly(vinyl amine)-*b*-poly(N-isopropylacrylamide-*stat*-N-vinyl carbazole) copolymer was synthetized by replacing the PNIPAM second block with a statistical copolymerization of NIPAM and NVC to target $PVAm_{10}$-*b*-P($NIPAM_{0.92}$-*stat*-$NVC_{0.08}$)50 containing 8% mol. of NVC in the second block (Scheme SI1). This diblock copolymer was synthesized to allow the monitoring of grafting

of the copolymer onto the nanoparticles surface. First, according to Suchao-in *et al.*,[33] a statistical polymerization of NIPAM and NVC in the presence of a $PVPI_{10}$-X macro-RAFT agent afforded the final PVPI-*b*-P(NIPAM-*stat*-NVC)-X. Monomer conversions were nearly quantitative (> 97%) after 16 hours as expected from the literature of statistical copolymerization of NIPAM and NVC.[33] The resulting polymer was characterized by SEC and had a $M_{n,\mathrm{MALS}}$ of 10000 g mol^{-1} and dispersity of 1.4 (Table 1-Entry 3). Chain extension was confirmed by SEC analysis, with similar presence of a fraction of unreacted first block in final block copolymer (Fig. SI5). We did not calculate the fraction of unreacted macro-CTA the way we did for the PVPI-PNIPAM copolymer. However, based on the relative contributions of the two populations on SEC chromatograms, the amount of PVPI homopolymer in both diblocks looks approximatively the same. ^{1}H NMR spectrum (Fig. SI6) of PVPI-*b*-P($NIPAM_{0.92}$-*stat*-$NVC_{0.08}$) allowed the determination of the copolymer composition of both blocks, which was 18:82, as expected from the theoretical composition (17:83). The post-polymerization treatment of PVPI-*b*-P($NIPAM_{0.92}$-*stat*-$NVC_{0.08}$) that includes the removal of the terminal xanthate functionality and the hydrazinolysis of PVPI block was performed with the same procedure than the one previously described. Finally, copolymer PVAm-*b*-P($NIPAM_{0.92}$-*stat*-$NVC_{0.08}$) was obtained and its M_n value was estimated from NMR composition to M_n = 6600 g mol^{-1}.

Residual $PVAm_{10}$ was removed by dialysis against ultrapure water for both copolymers. Purified $PVAm_{10}$-*b*-$PNIPAM_{50}$ and $PVAm_{10}$-*b*-P(NIPAM-*stat*-$NVC)_{50}$ were used as such for the surface modification of composite silica/hydrogel nanoparticles.

3. Surface modification of core/shell nanoparticles with thermoresponsive copolymers

3.1. Investigation of optimum conditions for "grafting to" methodology

Surface modification of SiNP@CS/ALG nanoparticles was performed by a "grafting to" approach of the previously synthesized diblock copolymer. The functionalization occurs between carboxylic acid groups of the alginate outer layer and the amine groups of the poly(vinyl amine) block in presence of NHS/EDC coupling agent in DMSO. Considering the nanoparticles surface calculated from hydrodynamic diameter determined by DLS and with the hypothesis that a random coil of copolymer of this molecular weight (7700 g mol^{-1}) should have a gyration radius of 2-3 nm,[43] the maximal grafting density was approximated between 1 and 5 $\%_{wt}$ of copolymer with respect to the core/shell nanoparticles. To determine the optimum copolymer/particles ratio within this range, grafted particles were prepared with different polymer weight ratios from 0.5 $\%_{wt}$ to 5 $\%_{wt}$ This amount will be referred to as feed weight ratio (*fwr*), i.e the weight of copolymer initially brought to a known weight of nanoparticles. The feed weight ratio should in any case be assumed as the effectively grafted ratio, the latter will be

determined further in this study. First, to determine optimal feeding ratio, zeta potential and NMR T_2 relaxation measurements were performed at different feed weight ratios as plotted in Fig. 5.

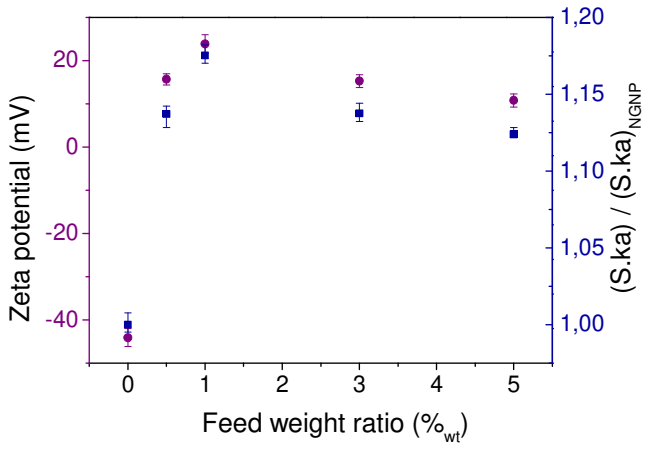

Fig. 5 Zeta-potential values and normalized surface. Ka ratios with respect to feed weight ratio during nanoparticles functionalization with $PVAm_{10}$-b-$PNIPAM_{50}$ copolymer in DMSO

T2 relaxation measurements are based on the difference of T2 values of the liquid at a solid interface (lower T2) versus the free liquid in bulk (higher T2). In the grafted/non-grafted nanoparticles system, lower T2 were expected when nanoparticles were grafted as the surface is sterically hindered and it is more difficult for water molecules around to interact with the surface. The comparison of grafted/non-grafted nanoparticles was achieved from S.Ka values, with the hypothesis that the undetermined surface S is constant and only Ka evolves in the process. $S.ka$ were obtained from NMR T_2 relaxation measurements using the following relationship : $\frac{1}{T_2} = S.ka.\varphi_p + \frac{1}{T_b}$ with T_2 the transverse relaxation time, S the surface area, ka the relaxativity coefficient, φ_p the particles volume fraction and Tb the relaxation time of the solvent. To determine S.Ka, T2 values were determined at several particle concentrations for each feed weight ratio from 0 to 5 %wt. Finally, results were plotted as S.Ka normalized by non-grafted nanoparticles $S.Ka_{NPNG}$.

Fig. 5 illustrates that both measurements, zeta potentials (left axis) and surface area measurements (right axis) evolved in the same trend with an optimum at 1% feed weight ratio. In the case of ζ-potential values, sign inversion occurred from negative non-grafted particles to positive surface when grafted from 0.5 to 5 % *fwr*. A maximum of 23.9 ± 2.1 mV was reached when *fwr* was 1%, followed by a slight decrease at higher *fwr*. Likewise, normalized S.Ka values rose to reach a maximum then decreased in the same trend as ζ-potentials. In both cases a plateau was expected more than a decrease as it was not expected that overcoming optimum *fwr* could inhibit grafting. From these consistent results, 1% *fwr* was still set as an optimal concentration and the following study focused on this ratio.

3.2. Diblock copolymer grafting: electrostatic or covalent interactions?

The "grafting to" strategy was also performed in aqueous medium. XPS analysis were carried to compare the influence of solvent conditions as well as evaluate the nature of the copolymer/particles interaction. To that purpose, survey scans were carried to identify the elements present in the system, followed by high resolution scans of the latters. Orbital deconvolution was achieved for a better understanding of the chemical environment of the extreme surface of our objects. This XPS study relies on the understanding of two phenomena occurring during the nanoparticles surface functionalization: i) a chemical modification with the intake of functional groups during the grafting and ii) a screening effect of the copolymer recovering the NPs surface. First a focus was held on surface modification in aqueous medium. Covalently (*GNP cov H_2O*) and electrostatically (*GNP ion H_2O*) grafted nanoparticles atomic compositions were compared to the bare nanoparticles (NGNP for non-grafted nanoparticles) (Table 2).

Table 2 XPS determination of atomic compositions and deconvolution ratios.

	Atomic compositions (%)				**Deconvolution ratios**			
	Si	*C*	*N*	*O*	*C-C / Si2p*	*N-C=O / Si*	*O-C=O / Si2p*	*C-N/Si2p*
NGNP	26	15	0	58	0,22	0.08	0.04	0.20
GNP cov H_2O	23	23	3	49	0,46	0.15	0.03	0.31
GNP cov DMSO	24	23	3	50	0,45	0.16	0.03	0.37
GNP ion H_2O	23	23	2	52	0,41	0.11	0.03	0.32
GNP ion DMSO	26	15	1	58	0,21	0.10	0.02	0.25

As shown in Table 2, the presence of $PVAm_{10}$-b-$PNIPAM_{50}$ copolymer induced a raise of global C atomic fraction because of the high content of carbon backbone in the thermosensitive copolymer, as well as a raise of N atomic fraction due to its high amine/amide content. After deconvolution, bond contributions were evaluated with respect to the Si2p fraction as the Si atomic composition is kept constant within the 10% error margin. More precisely, the C-C bond contribution doubled for both covalently and electrostatically modified nanoparticles, confirming the existence of a copolymer-based outer layer. The amide N-C=O bonding clearly rose during the grafting process as the copolymer contains amide in the PNIPAM block. The comparison between the covalent and ionic grafting in water does not allow a conclusion about the nature of interaction as both N-C=O/Si2p ratios are very close, 0.15 and 0.11 respectively.

Regarding surface modification in DMSO, the global content of C and N in *GNP cov DMSO* increased in the same trend as *GNP cov H_2O*, suggesting a similar grafting process. On the contrary, *GNP ion DMSO* C and N atomic composition, as well as bond-specific ratios were really close to *NGNP* which is no surprise as these conditions are unfavorable for electrostatic adsorption. In hindsight, XPS results tend

to highlight an efficient grafting but do not allow discussion about the nature of interaction between the NPs surface and the copolymer.

3.3. Grafting quantification

Quantification of thermoresponsive copolymer grafting was performed with spectrofluorimetry. Consistently with Perrier *et al*.'s work, $PVAm_{10}$-*b*-$P(NIPAM_{0.92}$-*stat*-$NVC_{0.08})_{50}$ copolymer is a fluorescent polymer which presented a 2-bands emission spectrum when excited at 325 nm (Fig.S7). First a calibration line of the normalized intensity at 346 nm was plotted against the concentration of $PVAm_{10}$-*b*-P(NIPAM-*stat*-$NVC)_{50}$ copolymer (Fig.S8). The calibration highlighted a quenching phenomenon above 5 µg/mL, meaning the range of linearity was between 0 and 27 A.U of normalized intensity. The linear relationship to obtain grafted copolymer concentration from fluorescence intensity was I_{346nm} = 5.32 C + 0.40 and was qualified with a 0.9997 R-squared value. The amount of grafted copolymer is determined by measuring I_{346nm} on a fluo-grafted NPs (FGNP) suspension, then calculating the concentration of copolymer and finally the weight ratio between copolymer and particles since the concentration of FGNP in suspension is known (0.5 mg mL^{-1}). In addition to XPS characterization, quantification of grafting was performed to compare the grafting medium (water or DMSO) and the nature of the grafting conditions (covalent or ionic). To this end, $PVAm_{10}$-*b*-P(NIPAM-*stat*-$NVC)_{50}$ copolymer was grafted i) in water in presence of coupling agents EDC/NHS (*FGNP cov* H_2O), ii) in water without coupling agents (*FGNP ion* H_2O), ii) in DMSO with coupling agents (*FGNP cov DMSO*) and finally iv) in DMSO without coupling agents (*FGNP ion DMSO*). The conditions without coupling agents were designed to evaluate electrostatic adsorption of the cationic copolymer onto the polyanionic surface of core/shell SiNP@CS/ALG nanoparticles. Fluorescently surface-modified nanoparticles suspensions at 0.5 mg mL^{-1} were characterized in the same conditions as calibration with resulting spectra depicted in Fig. 6.

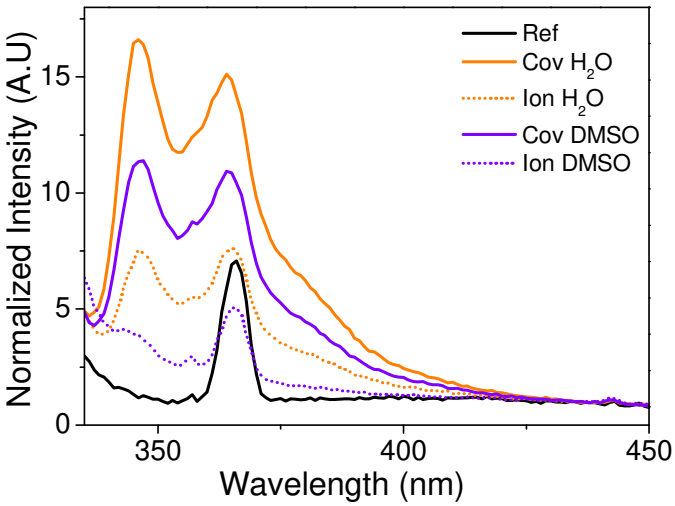

Fig. 6 Emission spectra after excitation at 325 nm of samples FGNP Cov H_2O, Ion H_2O, Cov DMSO, Ion DMSO and reference (non-fluo grafted nanoparticles) at 0.5 mg mL^{-1} in water

All spectra were normalized from baseline value at 435 nm as no emission is expected at this wavelength. Reference sample was a suspension of non-fluorescent GNP (NF-GNP) and presented a single band at 366 nm which was attributed to water Raman diffusion. Fluorescently grafted nanoparticles however displayed the same double-band spectra as the copolymer in solution, indicating its presence at the nanoparticles surface. The presence of coupling agents when performing grafting reaction clearly enhanced grafting as both conditions in water and DMSO showed better results. Effective grafting ratios were determined from the linear calibration and reported in Table 3.

Table 3 Quantification of grafting ratio from spectrofluorimetry calibration

	I 346 nm (A.U)	**C copo (µg mL^{-1})**	**r copo/par ($\%_{wt}$)**
NF-GNP	1.26	0.16	0.03
FGNP Cov H_2O	16.60	3.04	0.61
FGNP Ion H_2O	7.54	1.34	0.27
FGNP Cov DMSO	11.39	2.06	0.41
FGNP Ion DMSO	3.89	0.65	0.13

Covalent H_2O and DMSO samples contained respectively 0.61 and 0.41 % of copolymer in composite nanoparticles. Ionically modified nanoparticles had a 0.27 $\%_{wt}$ copolymer/particle ratio when the reaction occurred in water, i.e two times less than covalently modified nanoparticles in water. In condition A, as pH was only 6.1, this difference might be explained by the copolymer being only partly positively charged and thus less attracted to anionic SiNP@CS/ALG surface. Besides, electrostatic adsorption most probably occurred competitively to the covalent grafting reaction, meaning that covalent grafted ratio value contained also adsorption contribution. Electrostatic adsorption in DMSO did not succeed as expected in this aprotic solvent with a 0.13 % grafted ratio. As a conclusion and in

accordance with XPS results, whether the reaction is performed in water or in DMSO, the quantification proved that the use of coupling agents led to a more efficient grafting.

3.4. Study of colloidal stability

As the amount of copolymer grafted was quantified and results confirmed that a significant surface of nanoparticles should be covered from thermosensitive copolymer, the thermosensitivity of modified nanoparticles was investigated. $PVAm_{10}$-*b*-$PNIPAM_{50}$ diblocks are double-hydrophilic copolymers under cloud point temperature (Tc) and become amphiphilic above due to the hydrophobic character of PNIPAM above Tc. Consequently, the nanoparticles surface is expected to switch from a hydrophilic state to a hydrophobic shell above Tc. Stability studies were performed to evaluate whether on-demand hydrophobic behaviour of the nanoparticles surface would induce destabilization and flocculation phenomenon. First the range of thermosensitivity was determined by the physico-chemical characterization of $PVAm_{10}$-*b*-$PNIPAM_{50}$ copolymer. Cloud point temperature (Tc) was determined by turbidimetry and was 38.0 °C at 0.1 $\%_{wt}$ in water (Fig. SI9). Stability measurements of *GNP* nanoparticles suspensions at 10 mg mL^{-1} in NaCl 10^{-3} saline medium at pH 7 were performed with Turbiscan technology which is based on multiple light scattering. The particles stability was characterized using Turbiscan Stability Index (TSI) at T< Tc (25 °C) and T > Tc (45 °C) by comparing grafted (*GNP*) and non-grafted nanoparticles (*NGNP*) (Fig. 7). The higher TSI rises, the more unstable the suspension is.

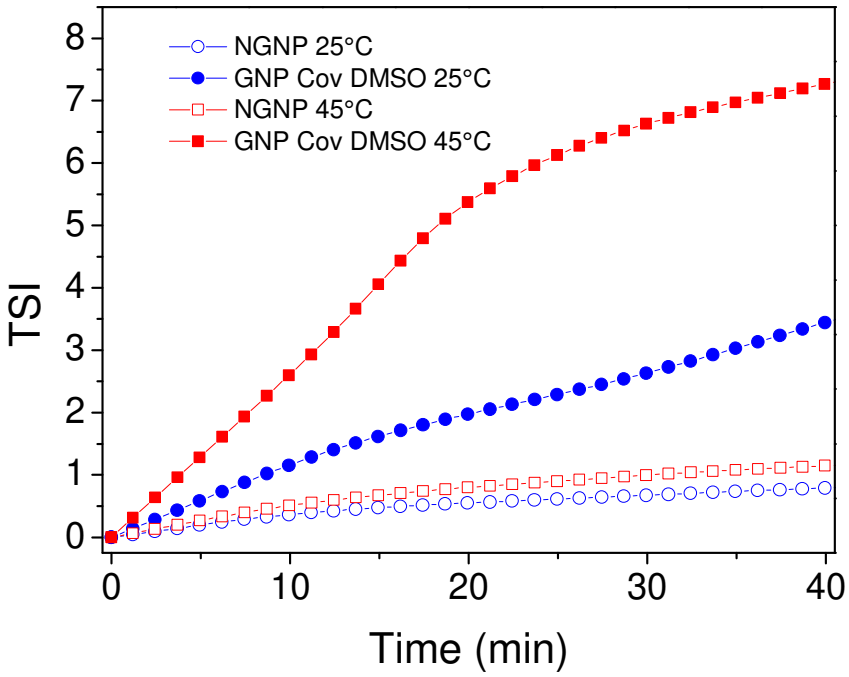

Fig. 7 Turbiscan Stability Index evolution with time of grafted (plain symbols) and non-grafted (hollow symbols) nanoparticles suspensions at pH 7 and temperature of 25 °C (circles) and 45 °C (squares)

First, TSI evolution of non-grafted nanoparticles samples confirmed that unmodified particles are not thermosensitive as expected as no significant differences were observed at 25 °C and 45 °C. Surface-modified nanoparticles at 25 °C exhibited lower stability than bare core/shell nanoparticles which could be explained by the screening of repulsive charges at the surface of core/shell particles (Fig. 1a, -20 mV) by PVAm-*b*-PNIPAM copolymer which is close to pKa at pH 7 and thus mainly neutral. At 45 °C, thermosensitively-modified nanoparticles effectively underwent rapid destabilization and reached a TSI over 7 after 40 min, flocculation and precipitation were macroscopically observed. The substantial difference in TSI between modified nanoparticles at 25 °C and 45 °C highlighted the thermosensivity of such suspensions. The observed destabilization effect comes from the nature of the LCST PNIPAM-based copolymer which is attached to the surface. Below Tc, copolymer chains are hydrophilic and extended around nanoparticles. As temperature rises and reaches the transition regime of thermosensitive diblock, water becomes a poor solvent for PNIPAM block, hydrogen bonds are broken and the copolymer undergoes conformational changes. Coil to globule transition occurs, PNIPAM exposes at the water interface its hydrophobic parts (backbone) conferring to the nanoparticles surface a hydrophobic character. Nanoparticles with hydrophobic surfaces in water tend to self-aggregate because of inter-chain hydrophobic interaction.[20] This self-association behaviour, resulting in flocculation and precipitation of the nanoparticles, was only observed in the modified

nanoparticles. This property could be used to generate an injectable drug delivery system which self-assembles in response to a physical stimulus such as temperature. Such *in situ*-formed particles assemblies is a very interesting tool for regenerative medicine and tissue engineering. Indeed, particle assemblies constitute mini invasive systems that can be easily implanted, optimally fits into a defect, and lead to a percolated network *in vivo* that can deliver, with kinetic and spatial control, active molecules such as growth factors.

Conclusion

A double-hydrophilic thermoresponsive diblock copolymer, PVAm-*b*-PNIPAM, was successfully synthesized by a two-step RAFT polymerization involving *N*-vinylphthalimide monomer followed by post-modification. Submicron core-shell nanoparticles were obtained from the *layer-by-layer* coating of silica nanoparticles with two natural oppositely-charged polyelectrolytes, chitosan and sodium alginate. The surface modification of these SiNP@CS/ALG nanoparticles relied on a 'grafting to' strategy of the thermoresponsive copolymer onto the alginate outer layer. First, the optimum feed weight ratio was determined to be $1\%_{wt}$ by a combined approach of zeta potential and T2 relaxation time measurements. Original copolymer PVAm-*b*-P(NIPAM-*stat*-NVC) was synthetized to monitor grafting reaction thanks to its fluorescence properties. A quantification study carried out by spectrofluorimetry revealed that the grafting efficiency could reach 60 % when performed in water. Characterizations highlighted that both covalent grafting and electrostatic adsorption occurred in water when the copolymer was in presence of the nanoparticles. Finally, thermosensivity properties study confirmed that this system enabled a temperature-triggered destabilization of the particles suspension at 45 °C. Such interesting properties represent a promising tool for regenerative medicine, tissue engineering as well as drug delivery. Indeed, this smart system has exciting prospects in the field of controlled drug delivery as the silica core could easily be replaced by a mesoporous silica core that would be used as drug nanocarrier.

Acknowledgement

The authors would like to thank Benoit Maxit (Cordouan Technologies) for T2 NMR measurements and Serife Korkmaz (Formulaction) for Turbiscan analysis.

References

[1] R. Roux, C. Ladavière, A. Montembault, T. Delair, Particle assemblies: Toward new tools for regenerative medicine, Mater. Sci. Eng. C. 33 (2013) 997–1007. https://doi.org/10.1016/j.msec.2012.12.002.

[2] N. Sahiner, S. Sagbas, N. Aktas, Preparation of macro-, micro-, and nano-sized poly(Tannic acid) particles with controllable degradability and multiple biomedical uses, Polym. Degrad. Stab. 129 (2016) 96–105. https://doi.org/10.1016/j.polymdegradstab.2016.04.010.

[3] J.K. Sahoo, M.A. VandenBerg, M.J. Webber, Injectable network biomaterials via molecular or colloidal self-assembly, Adv. Drug Deliv. Rev. 127 (2018) 185–207. https://doi.org/10.1016/j.addr.2017.11.005.
[4] Z. Shariatinia, Big family of nano- and microscale drug delivery systems ranging from inorganic materials to polymeric and stimuli-responsive carriers as well as drug-conjugates, J. Drug Deliv. Sci. Technol. 66 (2021) 102790. https://doi.org/10.1016/j.jddst.2021.102790.
[5] Y. Wang, Z. Li, Q. Hu, Emerging self-regulated micro/nano drug delivery devices: A step forward towards intelligent diagnosis and therapy, Nano Today. 38 (2021) 101127. https://doi.org/10.1016/j.nantod.2021.101127.
[6] X. Fu, L. Hosta-Rigau, R. Chandrawati, J. Cui, Multi-Stimuli-Responsive Polymer Particles, Films, and Hydrogels for Drug Delivery, Chem. 4 (2018) 2084–2107. https://doi.org/10.1016/j.chempr.2018.07.002.
[7] M. Alsehli, Polymeric nanocarriers as stimuli-responsive systems for targeted tumor (cancer) therapy: Recent advances in drug delivery, Saudi Pharm. J. 28 (2020) 255–265. https://doi.org/10.1016/j.jsps.2020.01.004.
[8] M. Dinc, C. Esen, B. Mizaikoff, Recent advances on core–shell magnetic molecularly imprinted polymers for biomacromolecules, TrAC Trends Anal. Chem. 114 (2019) 202–217. https://doi.org/10.1016/j.trac.2019.03.008.
[9] D.J. Denmark, J. Bradley, D. Mukherjee, J. Alonso, S. Shakespeare, N. Bernal, M.H. Phan, H. Srikanth, S. Witanachchi, P. Mukherjee, Remote triggering of thermoresponsive PNIPAM by iron oxide nanoparticles, RSC Adv. 6 (2016) 5641–5652. https://doi.org/10.1039/C5RA21617F.
[10] H.Y. Yang, Y. Li, D.S. Lee, Multifunctional and Stimuli-Responsive Magnetic Nanoparticle-Based Delivery Systems for Biomedical Applications, Adv. Ther. 1 (2018) 1800011. https://doi.org/10.1002/adtp.201800011.
[11] Y. Lu, M. Ballauff, Thermosensitive core–shell microgels: From colloidal model systems to nanoreactors, Prog. Polym. Sci. 36 (2011) 767–792. https://doi.org/10.1016/j.progpolymsci.2010.12.003.
[12] B. Zhao, L. Zhu, Mixed Polymer Brush-Grafted Particles: A New Class of Environmentally Responsive Nanostructured Materials, Macromolecules. 42 (2009) 9369–9383. https://doi.org/10.1021/ma902042x.
[13] G. Decher, Fuzzy Nanoassemblies: Toward Layered Polymeric Multicomposites, Science. 277 (1997) 1232–1237. https://doi.org/10.1126/science.277.5330.1232.
[14] P. Du, X. Zhao, J. Zeng, J. Guo, P. Liu, Layer-by-layer engineering fluorescent polyelectrolyte coated mesoporous silica nanoparticles as pH-sensitive nanocarriers for controlled release, Appl. Surf. Sci. 345 (2015) 90–98. https://doi.org/10.1016/j.apsusc.2015.03.151.
[15] W. Feng, W. Nie, C. He, X. Zhou, L. Chen, K. Qiu, W. Wang, Z. Yin, Effect of pH-Responsive Alginate/Chitosan Multilayers Coating on Delivery Efficiency, Cellular Uptake and Biodistribution of Mesoporous Silica Nanoparticles Based Nanocarriers, ACS Appl. Mater. Interfaces. 6 (2014) 8447–8460. https://doi.org/10.1021/am501337s.
[16] Y.-J. Yang, X. Tao, Q. Hou, Y. Ma, X.-L. Chen, J.-F. Chen, Mesoporous silica nanotubes coated with multilayered polyelectrolytes for pH-controlled drug release, Acta Biomater. 6 (2010) 3092–3100. https://doi.org/10.1016/j.actbio.2010.02.042.
[17] R. Roux, C. Ladavière, A. Montembault, L. David, T. Delair, Shear thinning three-dimensional colloidal assemblies of chitosan and poly(lactic acid) nanoparticles, J. Phys. Chem. B. 117 (2013) 7455–7464. https://doi.org/10.1021/jp4017486.
[18] J.M. Van Doorn, J. Sprakel, T.E. Kodger, Temperature-Triggered Colloidal Gelation through Well-Defined Grafted Polymeric Surfaces, Gels. 3 (2017) 21. https://doi.org/10.3390/gels3020021.
[19] M.-Q. Chen, T. Serizawa, M. Li, C. Wu, M. Akashi, Thermosensitive Behavior of Poly(N-isopropylacrylamide) Grafted Polystyrene Nanoparticles, Polym. J. 35 (2003) 901–910. https://doi.org/10.1295/polymj.35.901.
[20] M.-Q. Zhu, L.-Q. Wang, G.J. Exarhos, A.D.Q. Li, Thermosensitive Gold Nanoparticles, J. Am. Chem. Soc. 126 (2004) 2656–2657. https://doi.org/10.1021/ja038544z.

[21] M. Heskins, J.E. Guillet, Solution Properties of Poly(N-isopropylacrylamide), J. Macromol. Sci. Part - Chem. 2 (1968) 1441–1455. https://doi.org/10.1080/10601326808051910.
[22] A.P. Constantinou, T.K. Georgiou, Thermoresponsive Multiblock Copolymers: Chemistry, Properties and Applications, in: Temp.-Responsive Polym., John Wiley & Sons, Ltd, 2018: pp. 35–65. https://doi.org/10.1002/9781119157830.ch2.
[23] Y. Chen, Y. Gao, L.P. da Silva, R. P. Pirraco, M. Ma, L. Yang, R. L. Reis, J. Chen, A thermo-/pH-responsive hydrogel (PNIPAM-PDMA-PAA) with diverse nanostructures and gel behaviors as a general drug carrier for drug release, Polym. Chem. 9 (2018) 4063–4072. https://doi.org/10.1039/C8PY00838H.
[24] D. Giaouzi, S. Pispas, PNIPAM-b-PDMAEA double stimuli responsive copolymers: Effects of composition, end groups and chemical modification on solution self-assembly, Eur. Polym. J. 135 (2020) 109867. https://doi.org/10.1016/j.eurpolymj.2020.109867.
[25] R. Pelton, Polyvinylamine: A Tool for Engineering Interfaces, Langmuir. 30 (2014) 15373–15382. https://doi.org/10.1021/la5017214.
[26] D.D. Reynolds, W.O. Kenyon, The Preparation of Polyvinylamine, Polyvinylamine Salts, and Related Nitrogenous Resins, J. Am. Chem. Soc. 69 (1947) 911–915. https://doi.org/10.1021/ja01196a052.
[27] P. Stiernet, M. Dréan, C. Jérôme, P. Midoux, P. Guégan, J. Rieger, A. Debuigne, Tailor-Made Poly(vinylamine)s via Thermal or Photochemical Organometallic Mediated Radical Polymerization, in: Revers. Deactiv. Radic. Polym. Mech. Synth. Methodol., American Chemical Society, 2018: pp. 349–363. https://doi.org/10.1021/bk-2018-1284.ch017.
[28] Y. Maki, H. Mori, T. Endo, Controlled RAFT Polymerization of N-Vinylphthalimide and its Hydrazinolysis to Poly(vinyl amine), Macromol. Chem. Phys. 208 (2007) 2589–2599. https://doi.org/10.1002/macp.200700330.
[29] Y. Maki, H. Mori, T. Endo, Controlled Synthesis of Alternating Copolymers by RAFT Copolymerization of N-Vinylphthalimide with N-Isopropylacrylamide, Macromol. Chem. Phys. 211 (2010) 1137–1147. https://doi.org/10.1002/macp.200900544.
[30] Y. Maki, H. Mori, T. Endo, Synthesis of Amphiphilic and Double-Hydrophilic Block Copolymers Containing Poly(vinyl amine) Segments by RAFT Polymerization of N-Vinylphthalimide, Macromol. Chem. Phys. 211 (2010) 45–56. https://doi.org/10.1002/macp.200900332.
[31] R. Kanto, R. Yonenuma, M. Yamamoto, H. Furusawa, S. Yano, M. Haruki, H. Mori, Mixed Polyplex Micelles with Thermoresponsive and Lysine-Based Zwitterionic Shells Derived from Two Poly(vinyl amine)-Based Block Copolymers, Langmuir. 37 (2021) 3001–3014. https://doi.org/10.1021/acs.langmuir.0c02197.
[32] G. Conzatti, F. Ayadi, S. Cavalie, N. Carrère, A. Tourrette, Thermosensitive PNIPAM grafted alginate/chitosan PEC, Appl. Surf. Sci. 467–468 (2019) 940–948. https://doi.org/10.1016/j.apsusc.2018.10.269.
[33] N. Suchao-in, S. Chirachanchai, S. Perrier, pH- and thermo-multi-responsive fluorescent micelles from block copolymers via reversible addition fragmentation chain transfer (RAFT) polymerization, Polymer. 50 (2009) 4151–4158. https://doi.org/10.1016/j.polymer.2009.06.047.
[34] X. Liu, O. Coutelier, S. Harrisson, T. Tassaing, J.-D. Marty, M. Destarac, Enhanced Solubility of Polyvinyl Esters in scCO2 by Means of Vinyl Trifluorobutyrate Monomer, ACS Macro Lett. 4 (2015) 89–93. https://doi.org/10.1021/mz500731p.
[35] A. Glaria, M. Beija, R. Bordes, M. Destarac, J.-D. Marty, Understanding the Role of ω-End Groups and Molecular Weight in the Interaction of PNIPAM with Gold Surfaces, Chem. Mater. 25 (2013) 1868–1876. https://doi.org/10.1021/cm400480p.
[36] W. Stöber, A. Fink, E. Bohn, Controlled growth of monodisperse silica spheres in the micron size range, J. Colloid Interface Sci. 26 (1968) 62–69. https://doi.org/10.1016/0021-9797(68)90272-5.
[37] P. Lagarrigue, J. Soulié, D. Grossin, A. Dupret-Bories, C. Combes, V. Darcos, Well-defined polyester-grafted silica nanoparticles for biomedical applications: Synthesis and quantitative characterization, Polymer. 211 (2020) 123048. https://doi.org/10.1016/j.polymer.2020.123048.

[38] L. Despax, J. Fitremann, M. Destarac, S. Harrisson, Low concentration thermoresponsive hydrogels from readily accessible triblock copolymers, Polym. Chem. 7 (2016) 3375–3377. https://doi.org/10.1039/C6PY00499G.
[39] D.A. Shirley, High-Resolution X-Ray Photoemission Spectrum of the Valence Bands of Gold, Phys. Rev. B. 5 (1972) 4709–4714. https://doi.org/10.1103/PhysRevB.5.4709.
[40] J.H. Scofield, Hartree-Slater subshell photoionization cross-sections at 1254 and 1487 eV, J. Electron Spectrosc. Relat. Phenom. 8 (1976) 129–137. https://doi.org/10.1016/0368-2048(76)80015-1.
[41] S. Sistach, M. Beija, V. Rahal, A. Brûlet, J.-D. Marty, M. Destarac, C. Mingotaud, Thermoresponsive Amphiphilic Diblock Copolymers Synthesized by MADIX/RAFT: Properties in Aqueous Solutions and Use for the Preparation and Stabilization of Gold Nanoparticles, Chem. Mater. 22 (2010) 3712–3724. https://doi.org/10.1021/cm100674p.
[42] V.H. Dao, N.R. Cameron, K. Saito, Synthesis of ultra-high molecular weight ABA triblock copolymers via aqueous RAFT-mediated gel polymerisation, end group modification and chain coupling, Polym. Chem. 8 (2017) 6834–6843. https://doi.org/10.1039/C7PY01410D.
[43] T.E. de Oliveira, C.M. Marques, P.A. Netz, Molecular dynamics study of the LCST transition in aqueous poly(N-n-propylacrylamide), Phys. Chem. Chem. Phys. 20 (2018) 10100–10107. https://doi.org/10.1039/C8CP00481A.

Figures caption

Tables